

Design for earthquake-resistant short RC structural walls

Nick St. Zygouris^{*1}, Gerasimos M. Kotsovos^{1a} and Michael D. Kotsovos^{2b}

¹Lithos Consulting Engineers, 34 Anagirountos Av. 16672, Vari, Greece

²Laboratory of Concrete Research, National Technical University of Athens, Greece

(Received March 19, 2014, Revised June 19, 2014, Accepted October 13, 2014)

Abstract. The application of the compressive force path method for the design of earthquake-resistant reinforced concrete structural walls with a shear span-to-depth ratio larger than 2.5 has been shown by experiment to lead to a significant reduction of the code specified transverse reinforcement within the critical lengths without compromising the code requirements for structural performance. The present work complements these findings with experimental results obtained from tests on structural walls with a shear span-to-depth ratio smaller than 2.5. The results show that the compressive force path method is capable of safeguarding the code performance requirements without the need of transverse reinforcement confining concrete within the critical lengths. Moreover, it is shown that ductility can be considerably increased by improving the strength of the two bottom edges of the walls through the use of structural steel elements extending to a small distance of the order of 100 mm from the wall base.

Keywords: earthquake-resistant design; compressive force path method; reinforced concrete; short walls; seismic performance

1. Introduction

For all types of structural walls, current code provisions for the design of earthquake-resistant reinforced concrete (RC) structures specify three types of reinforcement: (i) vertical reinforcement through the use of which it is intended to safeguard flexural capacity corresponding to load-carrying capacity at least equal to the design load; (ii) horizontal web reinforcement in an amount sufficient to prevent the occurrence of shear failure before flexural capacity is attained; and, (iii) stirrup reinforcement confining concrete along the two vertical edges of the wall so as to form boundary column (BC) elements (boundary elements at the end of the walls) capable of satisfying the code requirements for ductility. The above reinforcement arrangement, however, has a significant drawback: the dense spacing of the stirrups often results in reinforcement congestion within the BC elements and this may cause difficulties in concreting and, possibly, incomplete compaction of the concrete as stated in Salonikios *et al.* (1999).

More recently, although the need for these three types of reinforcement has been confirmed for the case of slender walls (walls with a shear span-to-depth ratio $a_v/d > 2.5$), it has been shown by

*Corresponding author, M.Sc., E-mail: nikos@lithos.com.gr

^aPh.D., E-mail: gtkotsov@gmail.com

^bProfessor, E-mail: mkotsov@central.ntua.gr

experiment that the stirrup reinforcement of the BC elements can be considerably reduced (by specifying a larger stirrup spacing within a significantly smaller critical length) without compromising the code requirements for structural performance (Kotsovos *et al.* 2011). This reduction has been achieved by designing the walls in accordance with the compressive force path (CFP) method and, hence, the results obtained from the tests can also be viewed as evidence of the validity of this method when applied for the design of earthquake-resistant slender walls.

The aim of the present work is to show that, by extending the use of the CFP method for designing earthquake-resistant short walls (walls with $a_v/d < 2.5$), the provision of stirrup reinforcement such as that specified by current codes for confining concrete within the BC elements is not a prerequisite for safeguarding the structural performance code requirements for the design of earthquake-resistant structures. The work is based on the comparative study of the results obtained from tests on walls under loading mimicking seismic action, with the specimens being designed in accordance with either the Eurocode 8 (2004) specifications for medium ductility (DCM) or the CFP method. All structural walls investigated have an aspect ratio of just over 1.35 and, unlike the amount and arrangement of the transverse reinforcement, their geometric characteristics and flexural reinforcement are the same. Although the effect on structural behaviour of placing confining reinforcement within the BC elements of short walls has formed the subject of already published experimental work, none of the specimens tested to date has been designed in accordance with the CFP method (Kuang and Ho 2008, Takahashi *et al.* 2013). Moreover, in some cases attention is focussed in a study of shear types of failure of walls in which the rotation of both ends is prevented (Hidalgo *et al.* 2002). The presentation and discussion of the results is preceded by a concise description of the CFP method, as the concepts which underlie it are in sharp contrast with current code tenets.

2. Cause of brittle failure

The concepts which underlie the CFP theory are fully described by (Kotsovos and Pavlovic 1999), therefore, only concisely discussed in what follows.

The CFP theory provides the basis for the implementation of the limit-state philosophy into the practical design of RC structures through (a) the identification of the regions that form the path along which the compressive forces developing within a structural element or structure under load are transmitted to the supports, and (b) the strengthening of these regions so as to impart to the element or structure the desired load-carrying capacity with sufficient ductility. The use of the name *compressive force path* is intended to highlight these two key features of the theory.

2.1 Simply supported beam

The modelling of a simply-supported beam is seminal for the application of the CFP theory in design, since it represents the portion of any structure comprising linear elements between points of zero bending moment (i.e., points of contra-flexure, hinges, or simple supports). Fig. 1 shows the model considered by this theory as the most suitable for providing a simplified, yet realistic, description of the physical state of a simply-supported beam-like element at its ultimate limit state

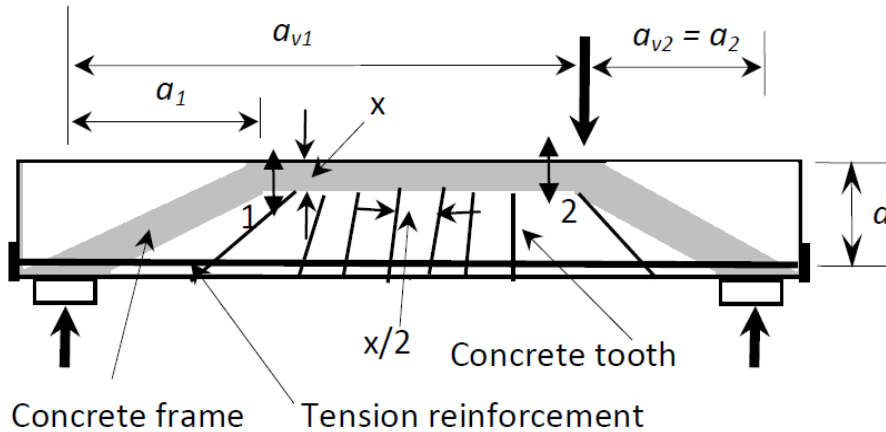


Fig. 1 Schematic representation of the physical state of a simply supported RC beam at its ultimate limit state

under the action of a transverse point load. Failure is considered to occur due to the development of transverse tensile stresses within the region of the path of the compressive force, the location of which depends on the value of the shear span-to-depth ratio (a_v/d), which affects the beam load-carrying capacity, the latter being expressed in a non-dimensional form as the ratio of the bending moment at failure, M_u , to the flexural capacity, M_f , in the manner indicated in Fig. 2 (Kotsovos and Pavlovic 1999). In fact, the trends exhibited by the variation of M_u/M_f with a_v/d correspond to four distinct types of structural element behaviour. Of these, types II and III are characterized by brittle, non-flexural modes of failure, whereas for types I and IV the structural element may be designed to exhibit ductile behaviour without the provision of transverse reinforcement in excess of a nominal amount (Kotsovos and Pavlovic 1999); hence the latter types of behaviour need no further discussion herein.

The brittle modes of failure associated with type II behaviour (encompassing, approximately, the range of a_v/d between 2.5 and 5) is caused by tensile stresses developing either in the region of change of the CFP direction (location 1 within shear span a_{v1} , in Fig. 1, assuming $a_{v1} > 2.5d$) or in the region of the cross section at the left-hand side of the point load, where the maximum bending moment combines with the shear force (location 2 within shear span a_{v1} , in Fig. 2). According to the CFP theory, the transverse stress resultant at **location 1** is numerically equal to the acting shear force, and, by invoking St Venant's principle, its effect spreads to a distance equal to the cross-section depth d , on either side of location 1, where the CFP changes direction. Moreover, it has been proposed⁸ that, for $N=0$, the value of the tensile force that can be sustained at this location can be realistically obtained by

$$T_{II,1} = 0.5 \cdot b \cdot d \cdot f_t \tag{1}$$

Where b and d are the width and depth of the cross-section and f_t the tensile strength of concrete. On the other hand, transverse tensile stresses within the compressive zone of the cross section where the maximum bending moment combines with the shear force (location 2 in Fig. 1) may develop due to the loss of bond between the longitudinal reinforcement and the surrounding concrete in the manner indicated in Fig. 3. The figure indicates a portion of the structural element between two cross-sections defined by consecutive cracks, together with the

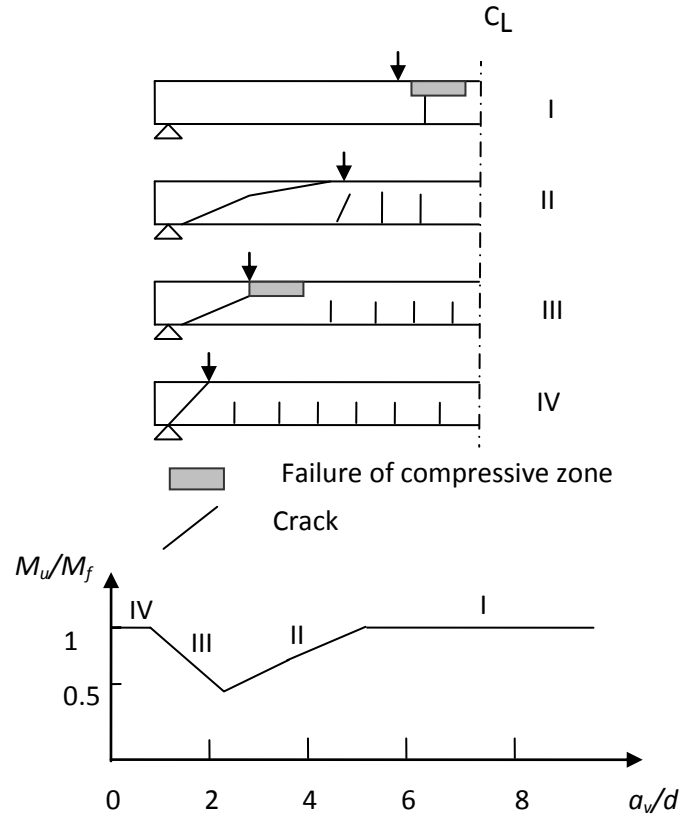


Fig. 2 Trends of behaviour exhibited by the relationship between load-carrying capacity (M_u/M_f) and span-to-depth ratio (a_v/d) and corresponding modes of failure

internal forces which develop at these cross-sections before and after the loss of bond τ necessary to develop due to the increase in tensile force ΔF_s . Setting the flexural moment $M=F \cdot z$ and observing that the shear force equals $V=dM/dx=(dF_s/dx) \cdot z+F_s \cdot (dz/dx)$, it can be seen that the two products on the right hand side of the equation correspond to beam (bond) and arch (no bond) action, respectively.

From the figure, it can be seen that the loss of bond may lead to an extension of the right-hand side crack and, hence, a reduction of the compressive zone depth (x), which is essential for the rotational equilibrium of this portion as indicated by the relation

$$F_c \cdot (x_l - x_r) / 2 = V \cdot (x_l / 2) \tag{2}$$

The reduction of the compressive zone depth increases the intensity of the compressive stress field, as compared to its value at the left-hand side of the portion, thus leading to dilation of the volume of concrete, which causes the development of transverse tensile stresses (σ_t in Fig. 3) in the adjacent regions. By considering these transverse tensile stresses and the ensuing triaxial stress conditions, it has been possible to express the shear force ($V_{II,2}$) that can be sustained at **locations 2** just before horizontal splitting of the compressive zone as follows (Kotsovos and Kotsovos 2008)

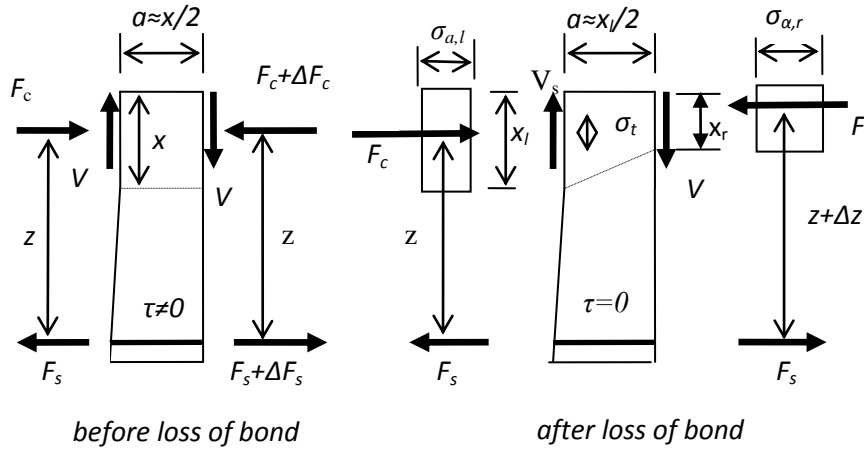


Fig. 3 Redistribution of internal actions in the compressive zone due to loss of bond between concrete and flexural reinforcement

$$V_{II,2} = F_c [1 - 1 / (1 + 5f_t / f_c)] \tag{3}$$

In contrast with type II behaviour, the brittle failure characterising type III behaviour (encompassing, approximately, the range of a_v/d between 1 and 2.5) is a flexural mode of failure caused by the loss of load-carrying capacity of the compressive zone (the depth of which decreases considerably due to the deep penetration of the inclined crack that forms within the shear span) before yielding of the tension reinforcement (see Fig. 2). For this type of behaviour the load-carrying capacity of an RC beam with a given value of a_v/d ranging between 1 and 2.5 (see shear span a_{v2} in Fig. 1) may be obtained by linear interpolation of the values of M_u/M_f corresponding to $a_v/d=1$, for which $M_u=M_f$ (see Fig. 2) and $a_v/d=2.5$, for which $M_u=V a_v$, where $V=\min(V_{II,1}, V_{II,2})$ with $V_{II,1}=T_{II,1}$ ^{7,8} (Kotsovos and Kotsovos 2008, Kotsovos 2014). With M_u known, the transverse reinforcement required to increase M_u to M_f is $A_{sv}=2(M_f-M_u)/(a_s f_{yv})$ uniformly distributed within a_v (Kotsovos and Kotsovos 2008).

2.2 Structural wall model

The physical model of the simply-supported beam shown in Fig. 1 can also be used to model a structural wall as illustrated in Figs. 4 and 5. Fig. 4 shows that the left-hand side (characterised by type II behaviour) of the simply-supported beam is equivalent to a slender cantilever subjected to a transverse point load near its free end, since the boundary conditions at the fixed end of the cantilever are similar to the conditions at the beam’s cross section through the load point. Similarly, Fig. 5 shows that the right-hand side (characterised by type III behaviour) of the simply-supported beam is equivalent to a short cantilever. Since a structural concrete wall under horizontal loading is essentially a cantilever beam, it can also be designed by adopting the CFP methodology. In fact, the application of this methodology to the design of slender structural

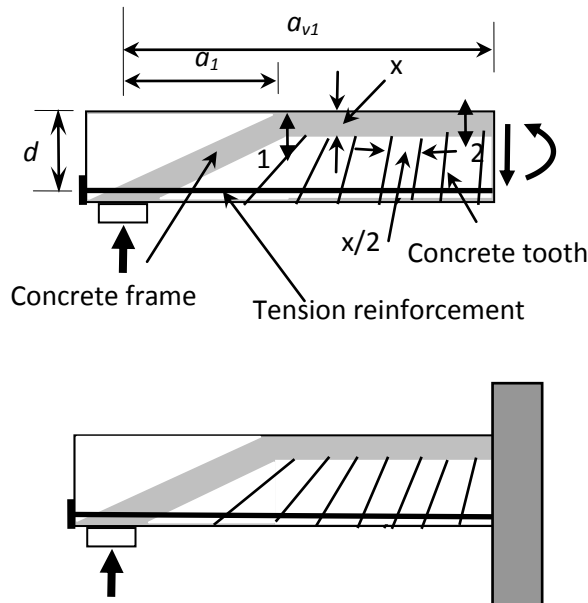


Fig. 4 Redistribution of internal actions in the compressive zone due to loss of bond between concrete and flexural reinforcement

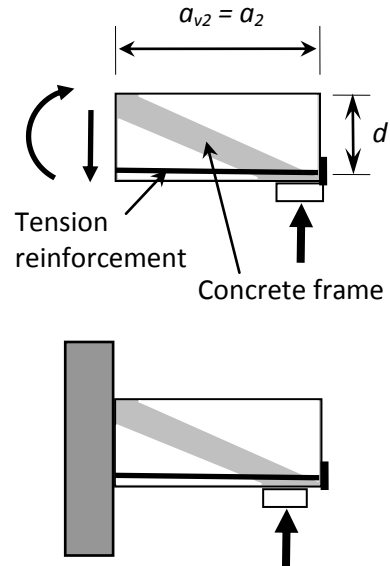


Fig. 5 Use of physical model of a simply supported beam of type III behaviour for modelling a cantilever

concrete walls been found to produce safe and efficient design solutions ((Kotsovos and Kotsovos 2008, Cotsovos and Kotsovos 2007), in spite of the considerably smaller amount of transverse reinforcement required in comparison with that specified by current codes.

3. Experimental programme

3.1 Design details

The structural walls investigated are designated by using a two part name, with the first part indicating the method of design (CFP, DCM, CFPU and CFPC) and the second the type of loading with '1' standing for type 1 and '2' for type 2 cyclic loading, where types of cyclic loading 1 and 2 are defined later.

The total number of walls tested is six; their design details are shown in Fig. 6 through to 9. The reinforcement details of specimens CFP-1 and CFP-2 (designed in accordance with the CFP method) are shown in Fig. 6, whereas those of specimens DCM-1 and DCM-2 (designed in compliance with EC2/8) are shown in Fig. 7. Specimens CFPU-2 and CFPC-2 were used in order to investigate the possibility of improving ductility beyond the code value specified. The design details of the latter specimens are similar to those of specimens CFP-1 and CFP-2 except for the bottom part of the walls' vertical edges. In this region, additional reinforcement, with a length equal to the depth of the compressive zone, is placed in the form of steel elements with a U-shaped

section (U65), for CFP-2 (see Fig. 8), and a pipe-like cylindrical section (CHS 49×4), for CFPC-2, the latter being free to slide within a cylindrical duct (CHS 60×5) encased into concrete, as indicated in Fig. 9. The figure also shows the sealant used to prevent the mortar from penetrating into the gap between the tube and the duct. The latter arrangement, known as “gap arrangement”, enables the free movement of the inner steel element, when the specimen edge is in tension; when the specimen edge is in compression, both the U and CHS elements were selected so as to be capable of compensating for the loss of strength of the compressive zone due to buckling of the longitudinal bars. Both the U and CHS steel elements have a yield stress of 235 MPa (S235).

All walls have length $l=1060$ mm, height $h=1200$ mm and width $b=150$ mm. With the exception of specimen DCM-1 which has three additional 10 mm diameter bars within the BC elements, since these formed part of the reinforcement grid used for confining concrete, the longitudinal reinforcement of all specimens (designated as $A_{s,v}$ in Table 1) comprises eleven pairs of 12 mm diameter steel bars at a centre-to-centre spacing of 100 mm, with the bars’ centre line lying at a distance of 15 mm from the closest wall face.

As for the longitudinal reinforcement, the amount of the horizontal web reinforcement (designated as $A_{s,h}$ in Table 1) is similar for all specimens; it comprises 8 mm diameter stirrups at a centre-to-centre spacing of 130 mm (5.11 in). However, for the DCM specimens additional reinforcement (designated as $A_{s,cc}$ in Table 1), in the form of 8 mm diameter stirrups at a 65 mm

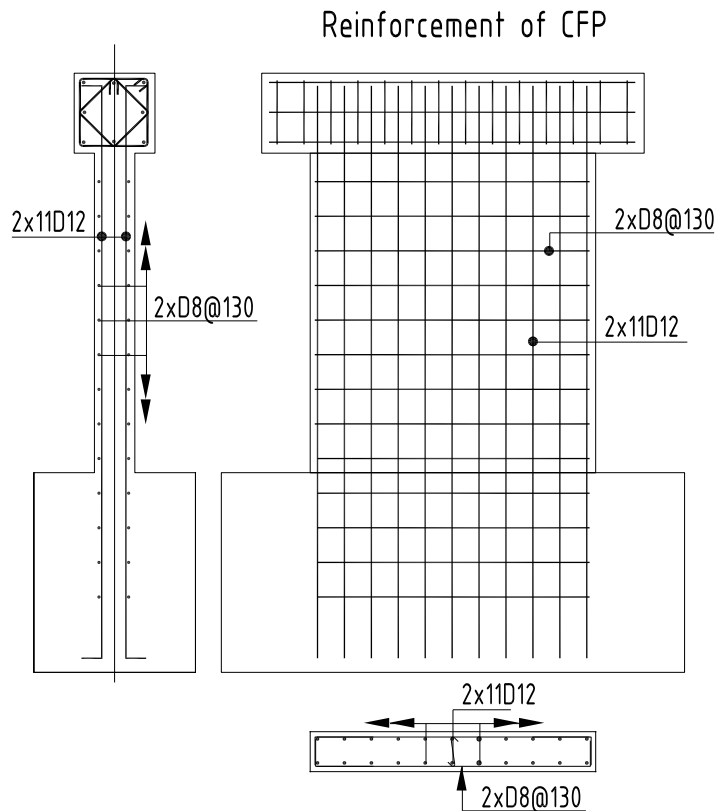


Fig. 6 Reinforcement details of walls CFP-1 and CFP-2

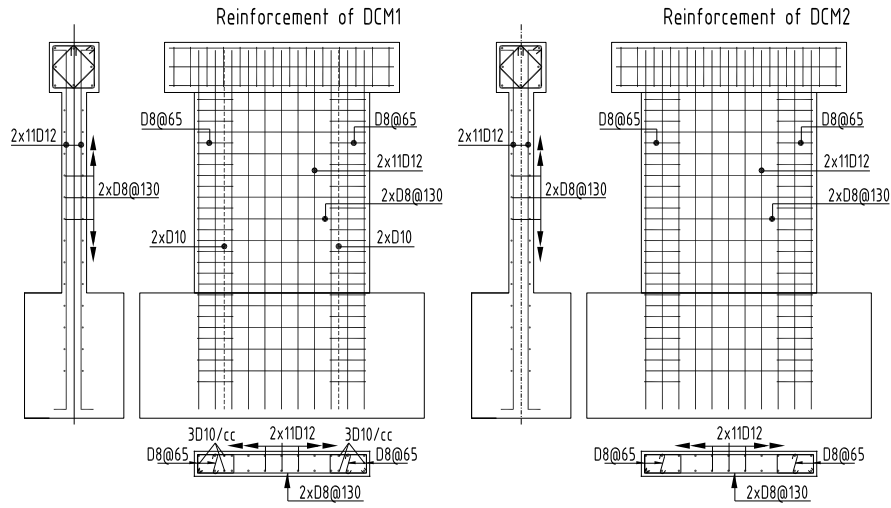


Fig. 7 Reinforcement details of walls DCM-1 and DCM-2

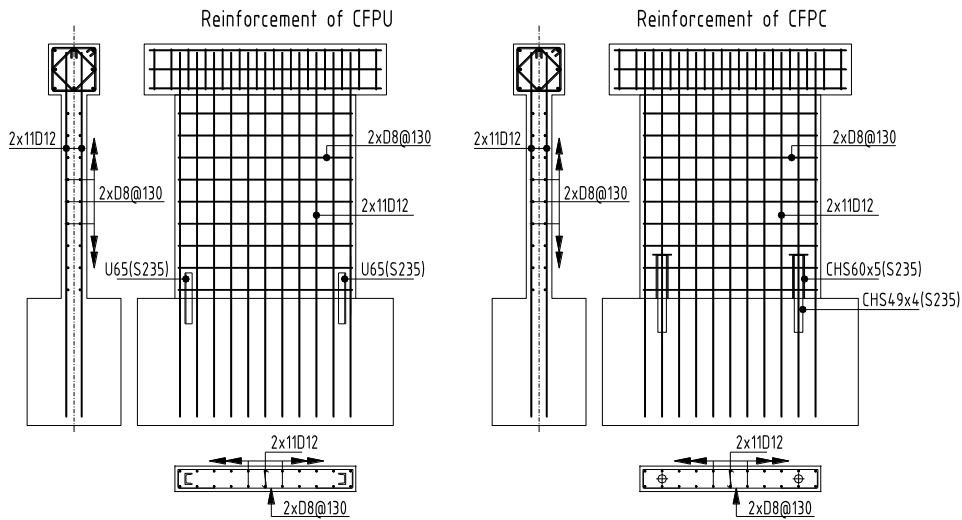


Fig. 8 Reinforcement details of walls CFPU and CFPC



Fig. 9 Detail of specimens CFPU-2 indicating the location of U65 steel element and CFPC-2 indicating the 'gap' arrangement

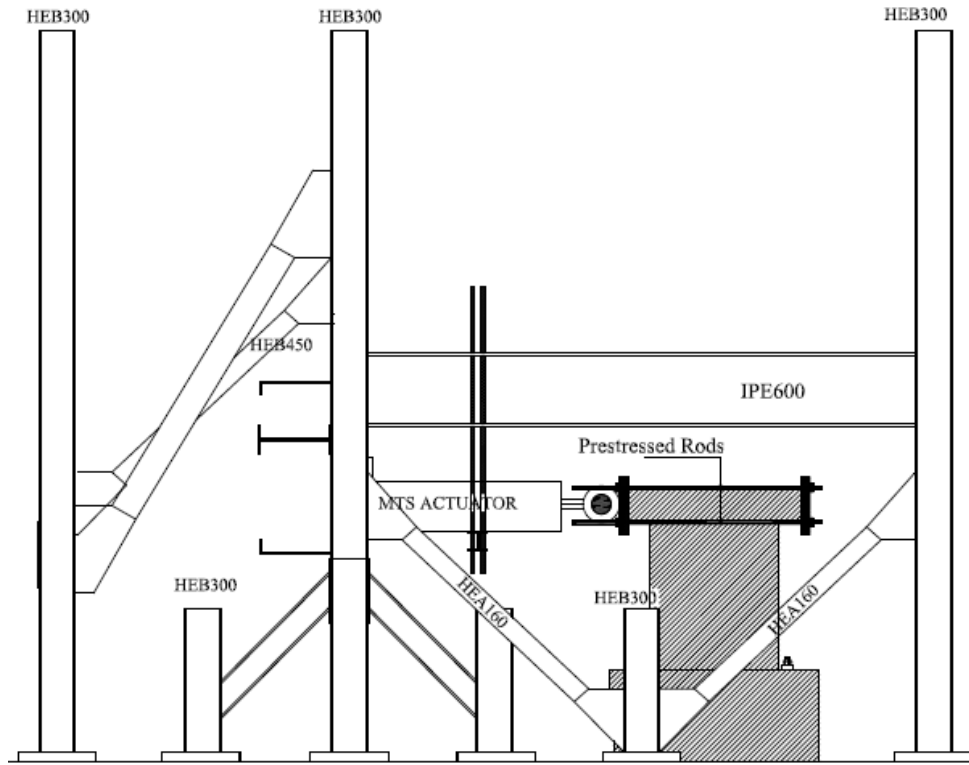


Fig. 10(a) Loading frame

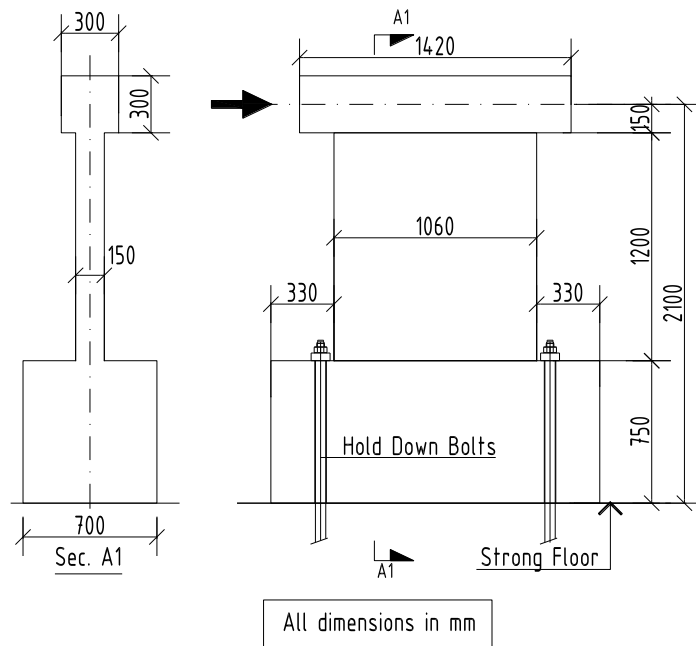


Fig. 10(b) Dimensions of specimens tested

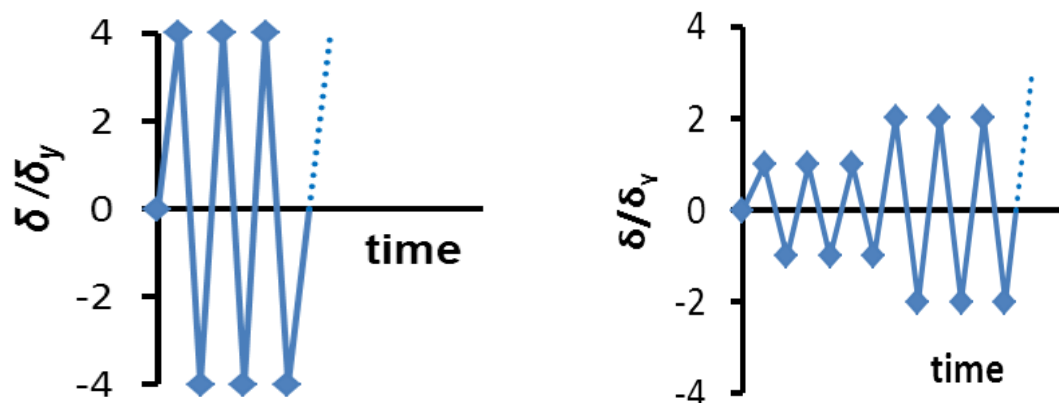


Fig. 11 Loading histories

Table 1 Conventional reinforcement of specimens

Specimen	A_{sv}	ρ_v (%)	A_{sh}	A_{sec}
CFP-1	2×(11D12)	1.55	2(D8@130)	-
CFP-2				
DCM-1	2×(11D12)+3D10 within each BC element	1.85	2(D8@130)	Φ8/65
DCM-2				
CFPU-2	2×(11D12)	1.55	2(D8@130)	
CFPC-2				

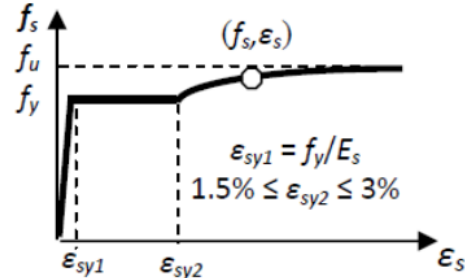
centre-to-centre spacing, is placed along the vertical edges of the walls in order to provide confinement to the BC elements. (It should be noted that the amount of transverse reinforcement specified by ACI 318-11 deviates only slightly from its counterpart specified by Eurocode 2/Eurocode 8; ACI specifies 8 mm at 100 mm spacing in the web and 5 mm diameter stirrups at 50 mm spacing in the boundary elements). For specimen DCM-1, the confining reinforcement within each BC element is provided in the form of a cage with three vertical 10 mm diameter bars placed at the middle of the stirrup legs closest to the wall faces. The presence of these vertical bars is allowed in the calculation of the wall's flexural capacity.

The details of the reinforcement used are summarized in Table 1, with the steel properties being provided in Table 2. The embodied steel sections have a nominal yield strength $f_y=235$ MPa. The concrete mixes used were commercial standard ready-mixes with a cylinder compressive strength at the time of testing $f_c=43$ MPa for CFP and DCM specimens and $f_c=20.4$ MPa for CFPU and CFPC specimens.

All specimens are monolithically connected to two 'rigid' prismatic elements at both their bottom and top faces. The specimens are fixed to the laboratory strong floor through the bottom prismatic element (1720 mm length x 750 mm height x 700 mm width) so as to simulate fixed-end conditions, whereas the load is applied through the top prismatic element (with square cross section of 300 mm side and 1420 mm length). Both prisms are over-sized and over-reinforced so to essentially behave as rigid bodies. The experimental set up constructed in order to carry out the tests is schematically depicted in Fig. 10.

Table 2 Yield and ultimate strength values for reinforcing bars and indicative stress strain diagram

Specimen	Diameter (mm)	f_y (MPa)	f_u (MPa)
CFP - DCM	8	563	563
	10	621	697
	12	600	726
CFPU - CFPC	8	563	563
	10	621	697
	12	550	650



3.2 Loading regimes

The walls are subjected to two types (1 and 2) of cyclic loading applied in the form of statically imposed horizontal displacements varying between extreme predefined values as schematically indicated in Fig. 11. For type 1 loading, the imposed displacements vary between values corresponding to ductility ratios of around ± 4 until failure occurs; failure is considered to occur when the sustained load becomes smaller than 80% the peak load value. For type 2 loading, the extreme predefined values of displacement are initially set to ± 10 mm (corresponding to ductility ratio of around ± 1) increasing in equal steps thereafter until failure (as defined above) of the specimens. Three load cycles are carried out for each of the above predefined values with a displacement rate of 0.25mm/s.

3.3 Design

The walls are designed so that their load-carrying capacity is reached when their base cross-section attains its flexural capacity, the latter condition being referred to henceforth as *plastic-hinge* formation. Using the cross-sectional and material characteristics of the walls and the rectangular stress block recommended in Kotsovos (2011), the flexural capacity M_f of the elements is calculated from first principles allowing for the contribution of all vertical reinforcement, both within the BC elements and within the web, and setting all material safety factors equal to 1. Using M_f , the wall load-carrying capacity P_f (and, hence, the corresponding shear force $V_f = P_f$) is easily calculated from static equilibrium. The values of M_f and $V_f = P_f$ for each of the specimens tested are given in Table 3 together with the experimentally-established values of the load-carrying capacity (P_u). The table also includes the values of bending moment M_y and load P_y which correspond at the yielding of the flexural reinforcement closest to the tensile face of the walls; the latter values are used for assessing the ductility ratio of the specimens tested.

For calculating the flexural capacity of specimens CFPU and CFPC, it was considered that the embodied steel sections contribute only when they are in compression and in that case the steel sections have common strains with the surrounding concrete.

As discussed earlier, the horizontal reinforcement of the walls is designed either in compliance with the earthquake-resistant design clauses of Eurocode 2 and Eurocode 8 or in accordance with the CFP method. From Figs. 6 and 7, it is interesting to note the densely spaced stirrups confining the BC elements within the “critical regions” (extending throughout the wall height) specified by the Codes. Such spacing, resulting from expression 5.20 of Eurocode 8 (clause 5.4.3.4.2), is

considered to safeguard ductile wall behaviour. As discussed in Section 1, in contrast with the code reasoning behind the calculation of the stirrups within the BC elements, the CFP method does not specify such reinforcement for structural elements, such as the walls investigated herein, exhibiting type III behaviour (Kotsovos and Pavlovic 1999).

On the other hand, the horizontal web reinforcement designed in compliance with the code requirements (see clauses 6.2 and 9.6 in EC2) is considered to improve the wall's shear capacity so as to prevent shear failure of the walls before their flexural capacity is exhausted. This reasoning is also in conflict with that underlying the design of the horizontal reinforcement within the wall web in accordance with the CFP method: in the latter case, horizontal reinforcement is designed to sustain the horizontal force required to develop in order to produce additional flexural resistance which, when added to the bending moment corresponding to structural member's load-carrying capacity in the absence of horizontal reinforcement, the resulting bending moment becomes equal to the flexural capacity M_f of the cross section (Kotsovos *et al.* 2011).

Since most experiments carried out to date have shown that failure of short walls is associated with the failure of the compressive zone, it is investigated whether an increase in the strength of the compressive zone can really lead to higher ductility and improved overall behaviour.

Bearing in mind that the extra steel at the lower edges contributes to load-carrying capacity only when it is in compression, the strength of the compressive zone is provided jointly by concrete, conventional longitudinal reinforcement and the embodied steel sections. In view of this, the corresponding strains are lower than those without the embodied steel elements and depend on the embodied steel element stiffness. It is expected, therefore, that the destruction of the compressive zone will be delayed and this will lead to an improvement of overall structural behaviour.

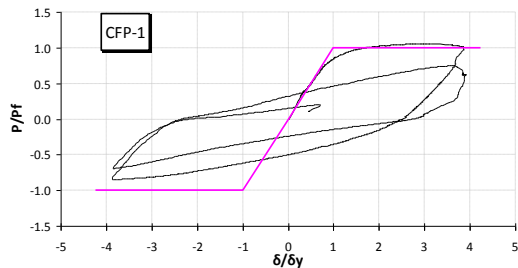


Fig. 12 Normalised load-top displacement curve for CFP-1 under loading type 1

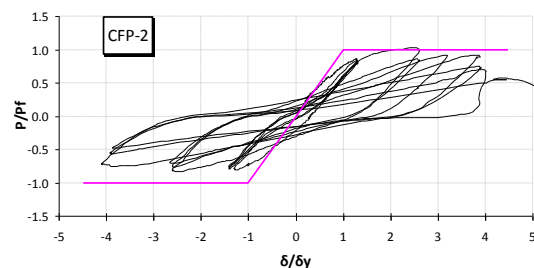


Fig. 13 Normalised load-top displacement curve for CFP-2 under loading type 2

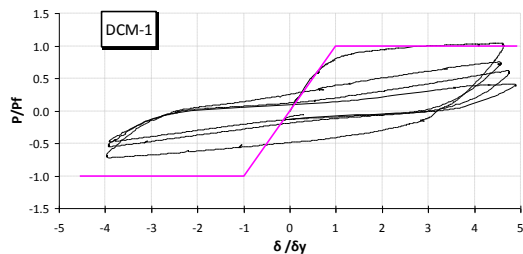


Fig. 14 Normalised load-top displacement curve for DCM-1 under loading type 1

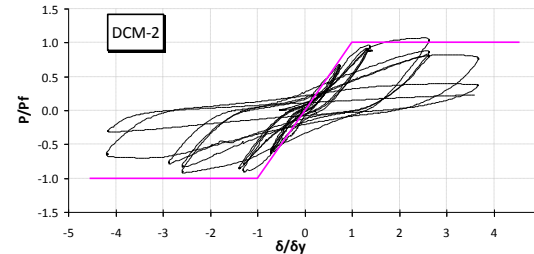


Fig. 15 Normalised Load-top displacement curve for DCM-2 under loading type 2

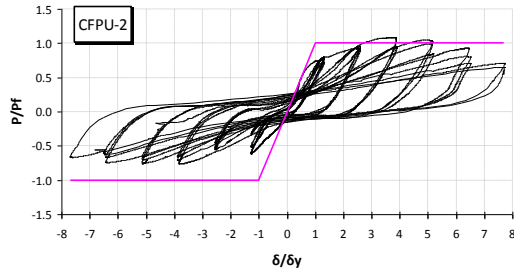


Fig. 16 Normalised load-top displacement curve for CFPU-2 under loading type 2

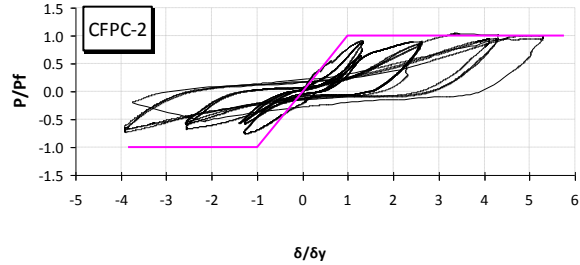


Fig. 17 Normalised load-top displacement curve for CFPC-2 under loading type 2

4. Results of tests

The main results of the work are given in Figs. 12 to 21 and Tables 3 and 4. Figs. 12 and 13 show the curves describing the relationship between applied load and horizontal displacement of the load point for the case of the CFP specimens under the two types of statically-applied cyclic loading, whereas their counterparts for the DCM, CFPU and CFPC specimens are shown in Figs. 14 and 15 and Figs. 16 and 17, respectively. All curves are shown in a normalised form by dividing the values of load with the calculated value of the load-carrying capacity P_f and the values of displacements with the calculated value of the displacement at nominal yield. Figs. 18 and 19 show the variation of the energy dissipated during each load cycle with increasing values of the ductility ratio, for the types of cyclic loading adopted for the tests. The dissipated energy during each cycle is provided in a form normalized with respect to a nominal value of the elastic energy expressed as $E_y = P_y \cdot \delta_y$. The backbone envelopes of the normalized load-displacement curves in Figs. 13, 15, 16 and 17 are shown in Fig. 20, with the modes of failure of the walls being depicted in Fig. 21. Finally, the calculated values of bending moment M_y and corresponding force P_y at yield, flexural capacity M_f and corresponding load-carrying capacity P_f , and the experimentally established values of load-carrying capacity P_u are given in Table 3, whereas Table 4 includes displacements $\delta_{y,n}$, δ_{sust} , δ_{fail} corresponding at nominal yield, sustained load cycle, and load cycle at

Table 3 Calculated values of bending moment M_y and corresponding force P_y at yield, flexural capacity M_f and corresponding load-carrying capacity P_f and experimentally-established values of load-carrying capacity P_{exp}

Specimen	Calculated values				Experimental Results	
	M_y (kNm)	P_y (kN)	M_f (kNm)	P_f (kN)	P_{max} (kN)	P_{max}/P_f
CFP-1	436	323.0	698	517.0	547.84	1.06
CFP-2	436	323.0	698	517.0	536.62	1.04
DCM-1	535	396.3	810	600.0	623.84	1.04
DCM-2	436	323.0	698	517.0	554.66	1.07
CFPU-2	385	285.2	607	449.6	491	1.09
CFPC-2	380	281.5	600	444.4	466	1.05

Table 4 Displacements $\delta_{y,n}$, δ_{sust} , δ_{fail} corresponding at nominal yield, sustained load cycle, and load cycle at failure, respectively, together with the values of the ductility ratio at the sustained load cycle (μ_{sust}) and the load cycle at failure (μ_{fail})

Specimen	$\delta_{y,n}$ (mm)	δ_{sust} (mm)	δ_{fail} (mm)	μ_{sust}	μ_{fail}
CFP-1	7.9	30.1	30.1	-	3.8
CFP-2		30.3	31.2	3.8	4.0
DCM-1	7.7	35.5	35.5	-	4.6
DCM-2		20.1	28.0	2.6	3.6
CFPU-2	7.9	50.0	60.0	6.3	7.6
CFPC-2		41.0	41.0	5.2	5.2

failure, respectively, together with the values of the ductility ratio at the sustained load cycle (μ_{sust}) and the load cycle at failure (μ_{fail}).

5. Discussion of results

From Figs. 1 and 2, it can be clearly seen that the walls designed in compliance with the EC2 and EC8 provisions differ from those designed in accordance with the CFP method in that the reinforcement of the former walls includes a dense stirrup arrangement within the BC elements extending throughout the height of the wall. It is reminded that, for all types of structural walls, current codes specify stirrups within the BC elements in order to provide confinement to concrete, since such confinement is considered essential for safeguarding adequate ductility for the walls. On the other hand, the provision of such reinforcement in accordance with the CFP method is deemed unnecessary for structural elements exhibiting type III behaviour (i.e., structural elements with a shear span-to-depth ratio $a_v/d \leq 2.5$ (Kotsovos and Pavlovic 1999, Kotsovos and Kotsovos 2008)). Such structural elements are the structural walls investigated in the present work since $a_v/d = 1350/636 \approx 2.12$, where d is the distance of the resultant of the forces developing in the tension reinforcement on account of bending from the extreme compressive fibre.

On the other hand, both the CFP and code methods specify transverse reinforcement in amounts sufficient to safeguard a flexural type of failure. However, as discussed in Section 2.3, the reasoning underlying these methods is different.

5.1 Type 1 cyclic loading

As indicated in Figs. 12 and 14 and Tables 3 and 4, the walls exhibited similar behaviour under this type of loading, in spite of the differences in the reinforcement arrangement. Wall DCM-1 exhibited a nearly 20% larger stiffness as well as sustained two additional load cycles before loss of load-carrying capacity, in spite of the larger imposed displacement corresponding to a ductility ratio of around 4.6. Such behaviour is attributed to the three additional 10 mm bars placed within each of the BC elements.

On the other hand, all walls exhibited a similar mode of failure in that the loss of load-carrying capacity is preceded by failure of the compressive zone at the wall base (see Fig. 21). Such behaviour clearly demonstrates that, under this type of loading, any amount of reinforcement larger

than that specified by the CFP method is essentially ineffective.

It is interesting to note in Table 3 that the deviation of the calculated values of load-carrying capacity from their experimentally-established counterparts is of the order of 4-9%. The former values of load-carrying capacity correspond to values of flexural capacity M_f calculated by assuming that, after yielding, the stress of the steel bars remains constant and equal to the yield stress f_y . The validity of this assumption is easily verified through a comparison of the calculated values of the steel strains corresponding to M_f with the maximum strain value of the yield plateau of the experimentally-established stress-strain curves of the steel used (see Table 2); such a comparison clearly demonstrates that the former values are smaller than the latter in all cases investigated. It appears, therefore, that ignoring the hardening properties of the steel is not, as usually suggested (Eurocode 8), the main cause of the above deviation and thus further work is required to clarify this matter.

However, although the calculated values of flexural capacity slightly underestimate their experimentally-established counterparts, the walls do exhibit a flexural mode of failure, as already discussed, and this is considered to be indicative of the conservative nature of the methods used to design the transverse reinforcement.

Figs. 12 and 14 and Table 4, also show the values of displacement at the nominal yield point used for assessing the specimens' ductility ratios. The location of the nominal yield point is determined in the manner described below:

(a) The cross section's bending moment at first yield, M_y (assessed by assuming that yielding occurs when either the concrete strain at the extreme compressive fibre attains a value of 0.002 or the tension reinforcement yields), and flexural capacity, M_f are first calculated.

(b) By using the values of M_y and M_f derived in (a), the corresponding values of the transverse load at yield, P_y , and at flexural capacity, P_f , are obtained from the equilibrium equations $P_y = M_y/a_v$ and $P_f = M_f/a_v$, where $a_v = 1350$ mm is the distance of the point of application of the applied load from the wall base.

(c) In Figs. 12 and 14 (first load cycle to peak load level), a line is drawn through the points of the load-displacement curves at $P=0$ and $P=P_y$. This line is extended to the load level P_f . The displacement $\delta_{y,n}$ corresponding to P_f is used to calculate the ductility ratios $\mu_{sust} = \delta_{sust}/\delta_{y,n}$ and $\mu_{fail} = \delta_{fail}/\delta_{y,n}$ in Table 4, where δ_{sust} and δ_{fail} are the values of displacement at the last sustained and final load cycles, respectively.

It is evident from the above that all specimens subjected to type 1 cyclic loading exhibited ductile behaviour. In fact, Table 4 indicates that the values of the ductility ratio (μ_{fail}) at the last load cycle of the specimens vary between 3.8 and 4.6.

From the energy dissipation plots in Fig. 18, it appears that the energy dissipated during the load-cycles leading to failure relates with the specimen load-carrying capacity: the higher a wall's load-carrying capacity (see Table 3) the larger the amount of the energy dissipated during the first post-peak load cycle. Such behaviour is considered to indicate that the horizontal reinforcement arrangement predominantly affects the post-peak structural characteristics. It may also be noted in the figure that the energy dissipated reduces with each additional load cycle.

5.2 Type 2 cyclic loading

From in Figs. 13 and 15, comparing the load-displacement curves shows that walls CFP-2 and DCM-2 exhibit similar behaviour, in spite of the presence of a significant amount of additional stirrup reinforcement within the BC elements of wall DCM-2. On the other hand, Figs. 16 and 17

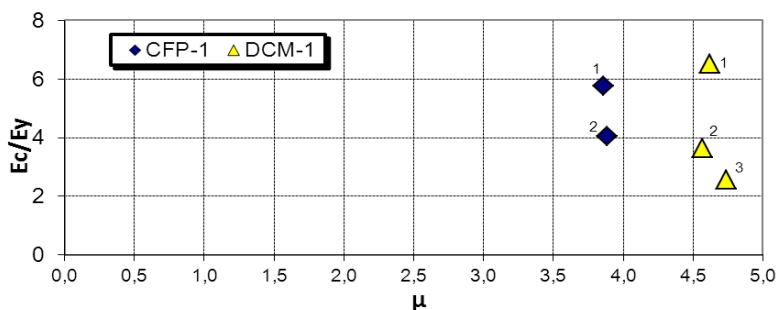


Fig. 18 Energy dissipated during the loading cycles leading to failure of the specimens under type 1 cyclic loading

clearly show that the presence of the additional steel element embedded at the bottom part of the specimens' vertical edges improves considerably the post peak structural behaviour. The values of the sustained ductility ratio for specimens CFPU-2 and CFPC-2 are 6.3 and 5.2, respectively, i.e., 64% and 36% larger than their counterparts for specimen CFP-2, whose conventional reinforcement is similar to that of specimens CFPU-2 and CFPC-2. Similarly, the values of the ductility ratio at failure for specimens CFPU-2 and CFPC-2 are 7.6 and 5.2, respectively, i.e., 92.5% and 62.5% larger than their counterparts for specimen CFP-2. It may also be noted that, in contrast with specimens CFP-2 and DCM-2, the residual load-carrying capacity of specimens CPFU-2 and CFPC-2 reduced below the code specified failure value of 80% the peak value in a controlled manner.

Fig. 19 shows the variation of the energy dissipated with successive load cycles corresponding to increasing values of the ductility ratio. The figure shows that, as for the case of the load-displacement curves, walls CFP-2 and DCM-2 exhibit similar trends of behaviour. After an initial slow rate of increase, the dissipated energy increases at an increasing rate up to the value of the ductility ratio essentially corresponding to the peak load level; thereafter, the rate of increase reduces and it appears that loss of load-carrying capacity occurs when the ability of the structural element to dissipate energy is diminished. In contrast with specimens CFP-2 and DCM-2, energy dissipation continues up to the last load cycle for specimens CFPU-2 and CFPC-2.

Moreover, as for the case of type 1 cyclic loading, the dissipated energy appears to reduce with successive load cycles corresponding to a given ductility ratio, for all walls investigated.

From Fig. 20, it appears that the backbone envelopes of the normalized lateral load-displacement curves of specimens CFP-2 and DCM-2 are identical; and this is considered as an indication of the insignificant effect of the reinforcement in excess of that specified by the CFP method on structural behaviour. The backbone curves for specimens CFPU-2 and CFPC-2 are also identical, but they differ from those of specimens CFP-2 and DCM-2, in that they are characterised by the formation of a "plateau" in the region of the peak load which extends to larger values of ductility.

The modes of failure of all specimens tested are depicted in Fig. 21. The figure shows that, in all cases, failure occurs due to failure of concrete under the compressive force developing on account of bending in one of the bottom edges of the specimens. Such a mode of failure is similar to that reported by Greifenhagen and Lstuzzi (2005) for the case of lightly reinforced squat walls which, however, in addition to the transverse cyclic loading, were also subjected to axial

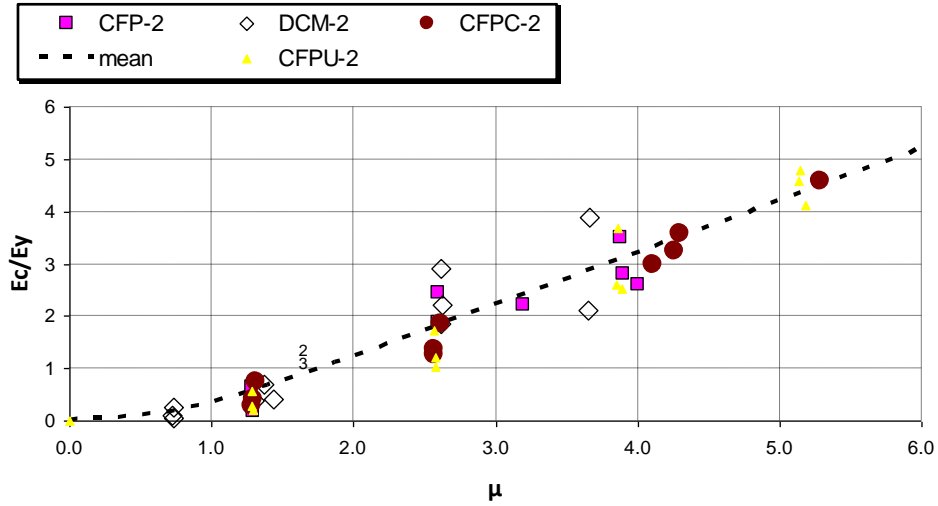


Fig. 19 Energy dissipated during the loading cycles leading to failure of the specimens under type 2 cyclic loading

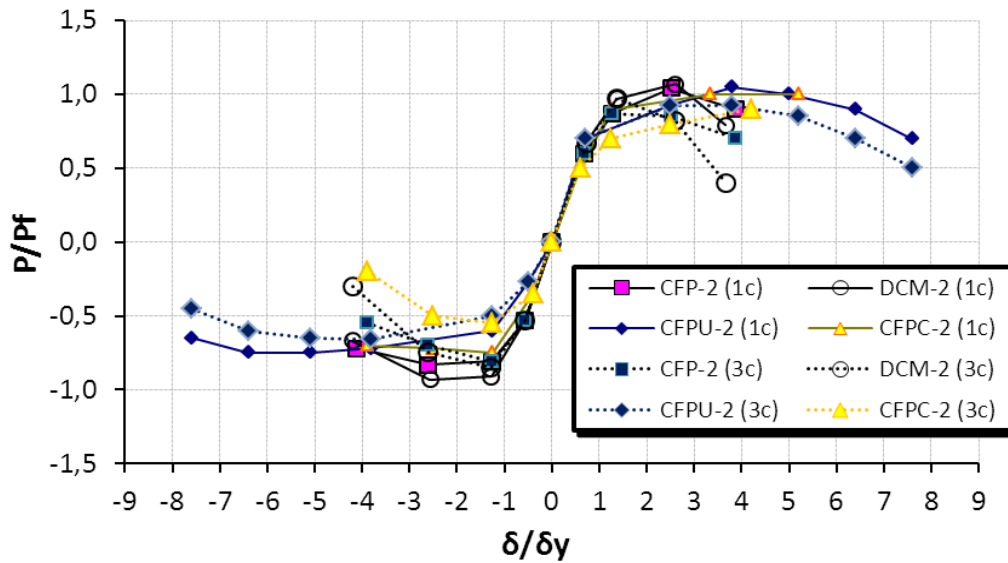


Fig. 20 Backbone envelopes of normalized lateral load-displacement curves corresponding to the peak load values of the first and third cycles to the predefined values of displacement

compression.

Failure of concrete in compression is followed by buckling of the vertical bars closest to the specimen edge, with the presence of the additional stirrups within the BC elements of walls DCM-2 reducing the rate of loss of load-carrying capacity. Specimens CFPU-2 and CFPC-2 are also characterised by failure of concrete in the compressive zone, but, in this case, buckling of steel is prevented by the stiff embedded steel elements.

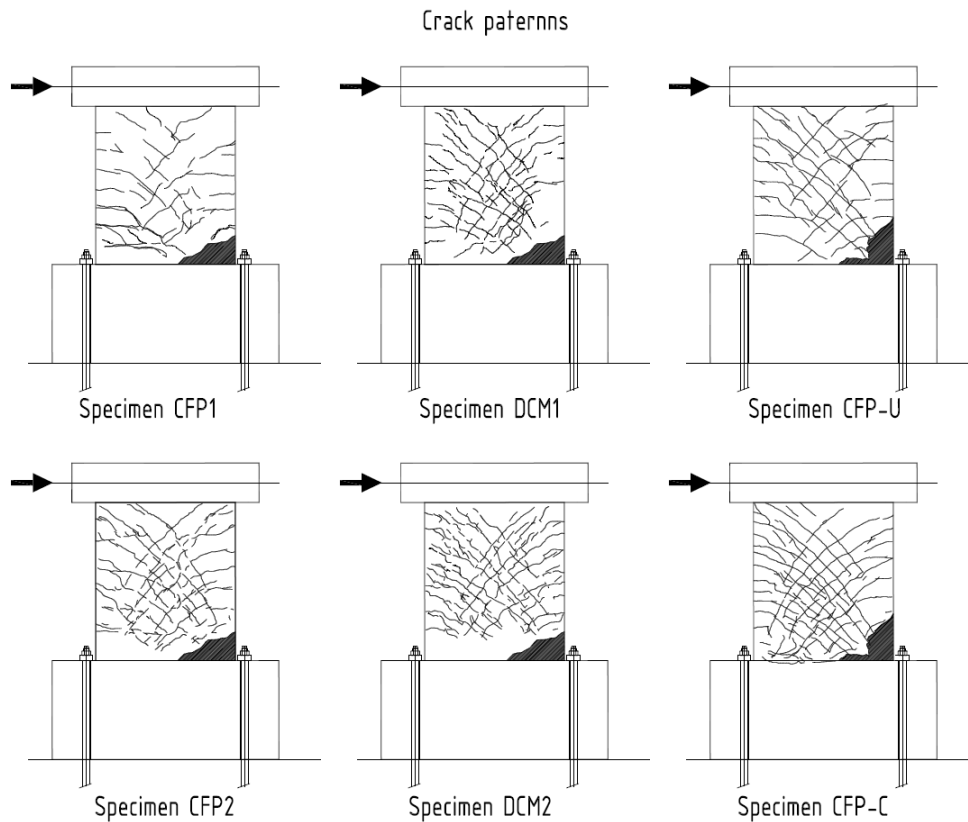


Fig. 21 Failure modes of the walls tested

6. Conclusions

Designing in accordance with the CFP method leads to significant savings in horizontal reinforcement without compromising the code performance requirements. This is because, in contrast with code specifications, the CFP method does not specify stirrups for the formation of BC elements along the edges of a short wall. As regards the web horizontal reinforcement all methods specified similar amounts for the walls investigated.

The reinforcement confining concrete within the BC elements appears to merely have a small effect on the post-peak characteristics of structural behaviour, in that they reduce the rate of loss of load-carrying capacity, well beyond the residual load-carrying capacity of 80% the peak load level specified by current codes as the limiting value for load-carrying capacity.

Reinforcing the bottom 200 mm long portion of the vertical edges of the walls with additional structural steel elements leads to a significant increase of the ductility ratio, prevents buckling of the vertical reinforcement and reduces damage of concrete in compression.

References

American Concrete Institute (2011), *Building Code Requirements for Structural Concrete (ACI 318-11)* and

- Commentary (ACI 318R-11).
- Eurocode 2 (2004), *Design of concrete structures, Part 1-1: General rules and rules of building*, British Standards.
- Eurocode 8 (2004), *Design of structures for earthquake resistance, Part 1: General rules, seismic actions and rules for buildings*, British Standards.
- Cotsovos, D.M. and Kotsovos, M.D. (2007), "Seismic design of structural concrete walls: an attempt to reduce reinforcement congestion", *Mag. Concrete Res.*, **59**(9), 627-637.
- Greifenhagen, C. and Lestuzzi, P. (2005), "Static cyclic tests on lightly reinforced concrete shear walls", *Eng. Struct.*, **27**, 1703-1712.
- Hidalgo, P.A., Ledezma, C.A. and Jordan, R.M. (2002), "Seismic behavior of squat reinforced concrete shear walls", *Earthq. Spectra*, **18**(2), 287-308.
- Kotsovos, G.M. (2011), "Assessment of the flexural capacity of RC beam/column elements allowing for 3D effects", *Eng. Struct.*, **33**(10), 2772-2780
- Kotsovos, M.D. (2014), *Compressive force-path method: Unified ultimate limit-state design of concrete structures*, Springer, Switzerland.
- Kotsovos, G.M., Cotsovos, D.M., Kotsovos, M.D. and Kounadis, A.N. (2011), "Seismic behaviour of RC walls: An attempt to reduce reinforcement congestion", *Mag. Concrete Res.*, **63**(4), 235-246.
- Kotsovos, M.D. and Pavlovic, M.N. (1999), *Ultimate limit-state design of concrete structures: A new approach*, Thomas Telford, London.
- Kotsovos, G.M. and Kotsovos, M.D. (2008), "Criteria for structural failure of RC beams without transverse reinforcement", *Struct. Eng.*, **86**(23/24), 55-61.
- Kuang, J.S. and Ho, Y.B. (2008), "Seismic behavior and ductility of squat reinforced concrete shear walls with nonseismic detailing", *ACI Struct. J.*, **105**(2), 225-231.
- Salonikios, T.N., Kappos, A.J., Tegos, I.A. and Penelis, G.G. (1999), "Cyclic load behavior of low-slenderness reinforced concrete walls: Design basis and test results", *ACI Struct. J.*, **96**(4), 649-660.
- Takahashi, S., Yoshida, K., Ichinose, T., Sanada, Y., Matsumoto, K., Fukuyama, H. and Suwada, H. (2013), "Flexural drift capacity of reinforced concrete wall with limited confinement", *ACI Struct. J.*, **110**(1), 95-104.

SA

Notations

BC	Boundary column elements, (boundary elements at the end of the walls
b	wall width
h	wall height
l	wall length
f_c	uniaxial cylinder compressive strength
f_y	yield stress of steel bar
M_f	flexural capacity of wall
M_y	bending moment of wall corresponding at first yielding (either concrete or reinforcing steel)
P_u	experimentally-established load-carrying capacity of wall
P_f	load-carrying capacity of wall corresponding to M_f
P_y	load corresponding to M_y
V_f	shear force corresponding to M_f
$\delta_{y,n}$	displacement at nominal yield

δ_{sust}	displacement at last sustained load cycle
δ_{fail}	displacement at final load cycle (failure)
μ_{sust}	ductility ratio corresponding to δ_{sust}
μ_{fail}	ductility ratio corresponding to δ_{fail}